TESS Data Release Notes:
Sector 9, DR12

Michael M. Fausnaugh, Christopher J. Burke
Kavli Institute for Astrophysics and Space Science, Massachusetts Institute of Technology, Cambridge, Massachusetts

Douglas A. Caldwell
SETI Institute, Mountain View, California

Jon M. Jenkins
Ames Research Center, Moffett Field, California

Jeffrey C. Smith, Joseph D. Twicken
SETI Institute, Mountain View, California

Roland Vanderspek
Kavli Institute for Astrophysics and Space Science, Massachusetts Institute of Technology, Cambridge, Massachusetts

John P. Doty
Noqsi Aerospace Ltd, Billerica, Massachusetts

Eric B. Ting
Ames Research Center, Moffett Field, California

Joel S. Villasenor
Kavli Institute for Astrophysics and Space Science, Massachusetts Institute of Technology, Cambridge, Massachusetts

April 11, 2019

Acknowledgements

This report is available in electronic form at
https://archive.stsci.edu/tess/

---

[1] https://archive.stsci.edu/missions/tess/doc/EXP-TESS-ARC-ICD-TM-0014.pdf
[2] https://archive.stsci.edu/kepler/manuals/KSCI-19081-002-KDPH.pdf

1 Observations

TESS Sector 9 observations include physical orbits 25 and 26 of the spacecraft around the Earth. The use of Camera 1 in attitude control was disabled at the start of both orbits due to strong scattered light signals. Data collection was paused for 1.18 days during perigee passage while downloading data. In total, there are 24.08 days of science data collected in Sector 9.

Table 1: Sector 9 Observation times

	UTC	TJD[a]	Cadence #
Orbit 25 start	2019-02-28 17:09:34	1543.21648	227348
Camera 1 guiding enabled	2019-03-01-06:00:00	1543.75080	227733
Orbit 25 end	2019-03-13 00:57:34	1555.54148	236222
Orbit 26 start	2019-03-14 05:19:34	1557.00080	237273
Camera 1 guiding enabled	2019-03-14-12:00:00	1543.75080	227733
Orbit 26 end	2019-03-25 23:21:33	1568.47481	245534

[a] TJD = TESS JD = JD - 2,457,000.0

The spacecraft was pointing at RA (J2000): 145.9071°; Dec (J2000): $-45.3044°$; Roll: 145.9163°. Two-minute cadence data were collected for 20,000 targets, and full frame images were collected every 30 minutes. See the TESS project Sector 9 observation page[3] for the coordinates of the spacecraft pointing and center field-of-view of each camera, as well as the detailed target list. Fields-of-view for each camera and the Guest Investigator two-minute target list can be found at the TESS Guest Investigator Office observations status page[4].

1.1 Notes on Individual Targets

Four very bright stars (Tmag $\lesssim 2$) with large pixel stamps were not processed in the photometric pipeline. Target pixel files with raw data are provided, but no light curves were produced. The affected TIC IDs are 31975064, 38877693, 238196512, and 438741592.

Two stars (Tmag $\lesssim 2$, 300015238 and 354825493) had very bright unresolved stars nearby (300015239 and 354825513 respectively). The contaminating flux for these objects is very large and the pipeline assigns them an incorrect photometric aperture. In general, the quality of the resulting photometry for such targets is expected to be poor in light of the contamination.

Six bright (Tmag $\lesssim 4.5$), saturated, bleeding targets (220393543, 269407223, 354825493, 385220745, 93549165, and 45696212) had apertures selected that did not fully capture the bleed trails.

---

[3]https://tess.mit.edu/observations/sector-9
[4]https://heasarc.gsfc.nasa.gov/docs/tess/status.html

1.2 Spacecraft Pointing and Momentum dumps

The reaction wheel speeds were reset with momentum dumps every 3.125 days. Figure 1 summarizes the pointing performance over the course of the sector based on Fine Pointing telemetry.

At the start of each orbit, the Earth was close to the boresight of Camera 1, and the level of scattered light was too high for meaningful guide star centroids to be measured. Guiding with Camera 1 was therefore disabled at these times, and attitude control was done using only inputs from Camera 4. When Camera 1 guiding was re-enabled, the spacecraft attitude shifted by a small amount, about 1 arc-second (0.05 pixels).
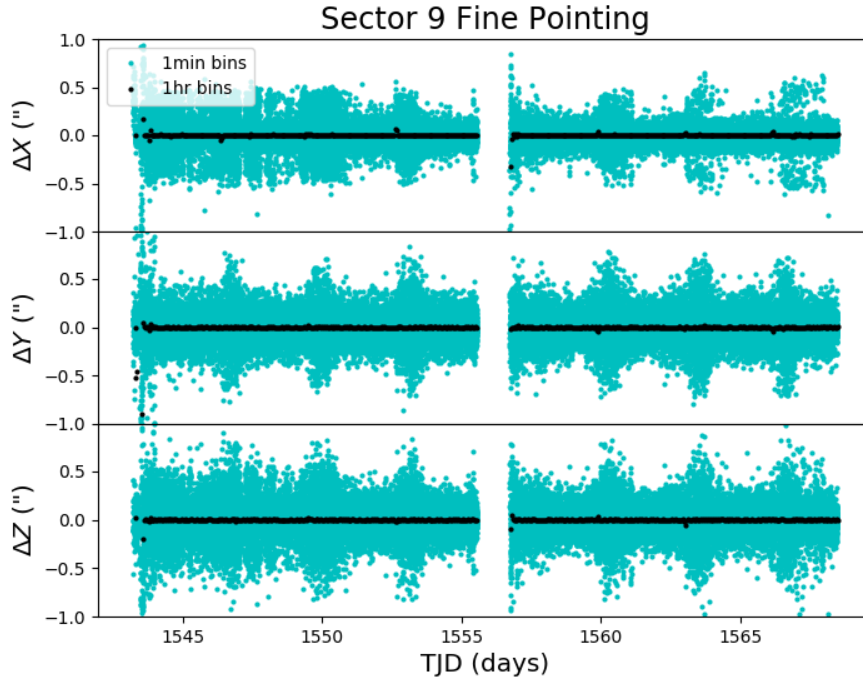

Figure 1: Guiding corrections based on spacecraft fine pointing telemetry. The delta-quaternions from each camera have been converted to spacecraft frame, binned to 1 minute and 1 hour, and averaged across cameras. Long-term trends (such as those caused by differential velocity aberration) have also been removed. The $\Delta X/\Delta Y$ directions represent offsets along the the detectors' rows/columns, while the ΔZ direction represents spacecraft roll.

1.3 Scattered Light

Figure 2 shows the median value of the background estimate for all targets on a given CCD as a function of time. Figure 3 shows the angle between each camera's boresight and the Earth or Moon—this figure can be used to identify periods affected by scattered light and the relative contributions of the Earth and Moon to the image backgrounds. In Sector 9, the main stray light features are caused by the Earth at the start of each orbit, and the Moon in Camera 1 in the first five days of orbit 26.
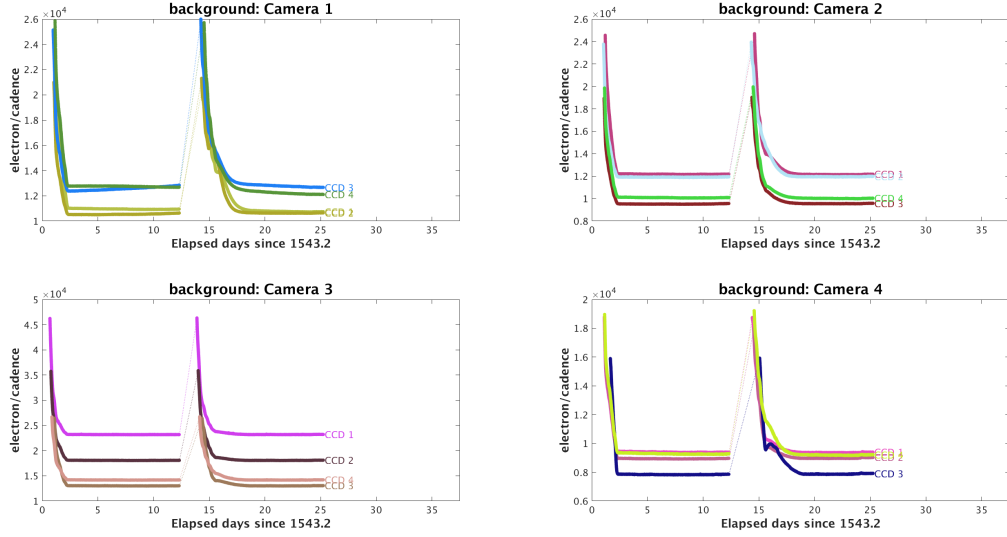
Figure 2: Median background flux across all targets on a given CCD in each camera. The changes are caused by variations in the orientation and distance of the Earth and Moon.

2   Data Anomaly Flags

See the SDPDD (§9) for a list of data quality flags and the associated binary values used for TESS data, and the Instrument Handbook for a more detailed description of each flag.

The following flags were not used in Sector 9: bits 1, 2, 7, 9, and 11 (Attitude Tweak, Safe Mode, Cosmic Ray in Aperture, Discontinuity, Cosmic Ray in Collateral Pixel).

Cadences marked with bits 3, 4, 6, and 12 (Coarse Point, Earth Point, Reaction Wheel Desaturation Event, and Straylight) were marked based on spacecraft telemetry.

Cadences marked with bit 5 and 10 (Argabrightening Events and Impulsive Outlier) were identified by the SPOC pipeline. Bit 5 marks a sudden change in the background measurements. In practice, bit 5 flags are caused by rapidly changing glints and unstable pointing at times near momentum dumps. Bit 10 marks an outlier identified by PDC and omitted from the cotrending procedure.

Cadences marked with bit 8 (Manual Exclude) are ignored by PDC, TPS, and DV for cotrending and transit searches. In Sector 9, these cadences were identified using spacecraft telemetry from the fine pointing system. All cadences with pointing excursions >21 arcseconds (∼1 pixel) were flagged for manual exclude. See Figure 4 for an assessment of the performance of the cotrending based on the final set of manual excludes.

In addition, strong scattered light signals affected the systematic error removal in PDC and the planet search in TPS. Cadences during this time were excluded from the pipeline analysis. The time periods for these exclusions are variable per CCD, and the corresponding cadence ranges are given in Table 2. Raw and flux-calibrated (without background correction) pixels for these cadences are provided in the target pixel files, but no photometry or centroid positions were calculated. The pipeline exports do not support data quality flags on a per CCD basis, and so the QUALITY column is not marked beyond the flags described
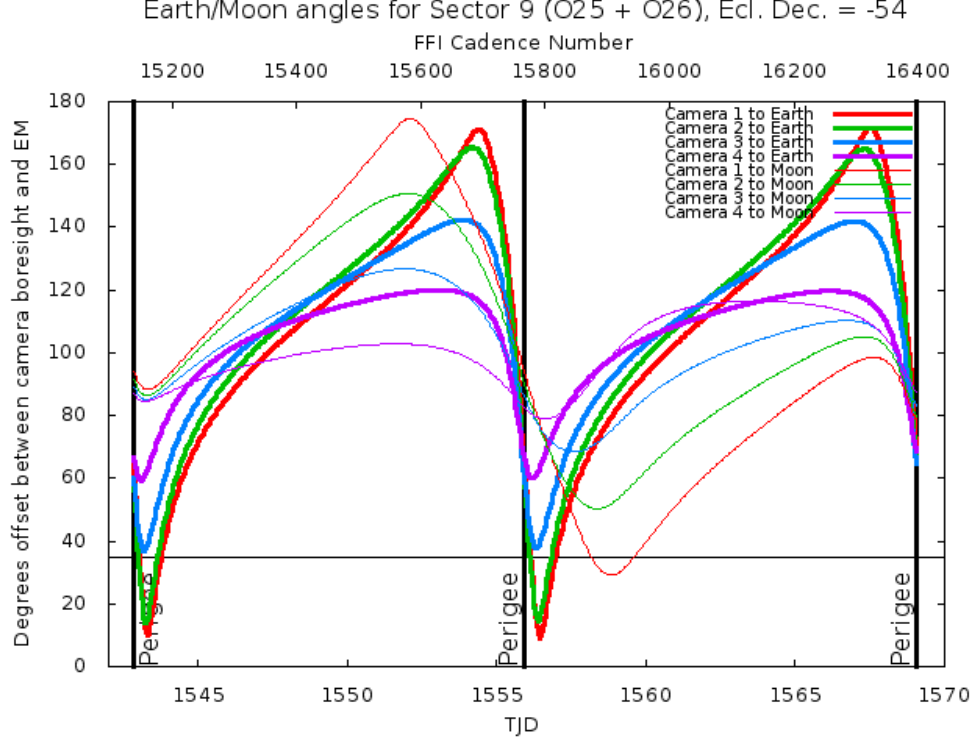
Figure 3: Angle between the four camera boresights and the Earth/Moon as a function of time. When the Earth/Moon moves within 37° of a camera's boresight, scattered light patterns and complicated features such as glints may appear. At larger angles, low level patchy features may appear. This figure can be used to identify periods affected by scattered light and the relative contributions of the Earth and Moon to the background. However, the background intensity and locations of scattered light features depend on additional factors, such as the Earth/Moon azimuth and distance from the spacecraft.

above.

FFIs were only marked with bits 6 and 12 (Reaction Wheel Desaturation Events and Straylight). Only one FFI is affected by each momentum dump.

3 Anomalous Effects

3.1 Smear Correction Issues

The following columns were impacted by bright stars in the science frame and/or the upper buffer rows, which bleed into the upper serial register resulting in an overestimated smear correction.

- Camera 1, CCD 3, Column 1427, Star Delta Crateris

- Camera 3, CCD 3, Column 332, Star Gamma Velorum

- Camera 2, CCD 4, Column 640, Star g Carinae

Table 2: Ranges for data excludes due to scattered light

Cam	CCD	Orbit 25	Orbit 26
1	1	227348–228224	237073–237882
1	2	227348–228108	237073–237653
1	3	227348–228061	237073–237605
1	4	227348–228179	237073–237814
2	1	227348–228215	237073–237863
2	2	227348–228104	237073–237654
2	3	227348–228144	237073–237691
2	4	227348–228169	237073–237774
3	1	227348–227851	237073–237352
3	2	227348–227913	237073–237434
3	3	227348–228144	237073–237687
3	4	227348–227979	237073–237528
4	1	227348–228156	237073–237720
4	2	227348–228186	237073–237819
4	3	227348–228547	237073–238196
4	4	227348–228176	237073–237841

In addition, Camera 3, CCD 3, Column 1356 is impacted by intra camera crosstalk from the bright star Gamma Velorum located on slice A impacting the same sub column on slice C (see Section 6.8.6 of the TESS instrument handbook).

3.2 Fireflies and Fireworks

Table 3 lists all firefly and fireworks events for Sector 9. These phenomena are small, spatially extended, comet-like features in the images that may appear one or two at a time (fireflies) or in large groups (fireworks). See the Instrument Handbook for a complete description.

Table 3: Sector Fireflies and Fireworks

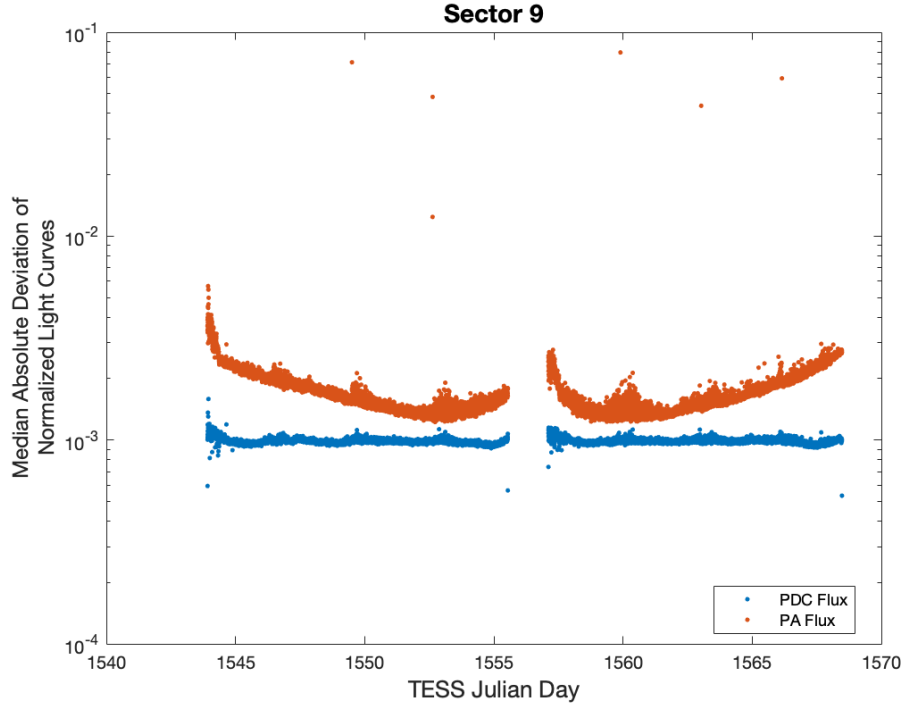| FFI Start	FFI End	Cameras	Description
2019066202934	2019066205934	1,2	Fireflies
2019071232934	2019071235934	1	Firefly
2019071235934	2019072002934	4	Firefly
2019074105934	2019074112934	1	Firefly
2019078105934	2019078112934	1	Firefly

Figure 4: Median absolute deviation (MAD) for the 2-minute cadence data from Sector 9, showing the performance of the cotrending after identifying Manual Exclude data quality flags. The MAD is calculated in each cadence across stars with flux variations less than 1% for both the PA (red) and PDC (blue) light curves, where each light curve is normalized by its median flux value. The scatter in the PA light curves is much higher than that for the PDC light curves, and the outliers in the PA light curves are largely absent from the PDC light curves due to the use of the anomaly flags. Note that the first and last cadences in each orbit are treated as gaps by PDC.

4 Pipeline Performance and Results

4.1 Light Curves and Photometric Precision

Figure 5 gives the PDC goodness metrics for residual correlation and introduced noise on a scale between 0 (bad) and 1 (good). The performance of PDC is very good and generally uniform over most of the field of view. Figure 6 shows the achieved Combined Differential Photometric Precision (CDPP) at 1-hour timescales for all targets.

4.2 Transit Search and Data Validation

In Sector 9, the light curves of 19996 targets were subjected to the transit search in TPS. Of these, Threshold Crossing Events (TCEs) at the 7.1σ level were generated for 900 targets.

The top panel of Figure 7 shows the distribution of orbital periods for the TPS TCEs found in Sector 9. There is a slight excess of TCEs at orbital periods of 10 days and 14 days. Figure 8 shows the number of TCEs at a given cadence that exhibit a transit signal—the spacing between peaks accounts for the preferred periods in Figure 7, and are associated
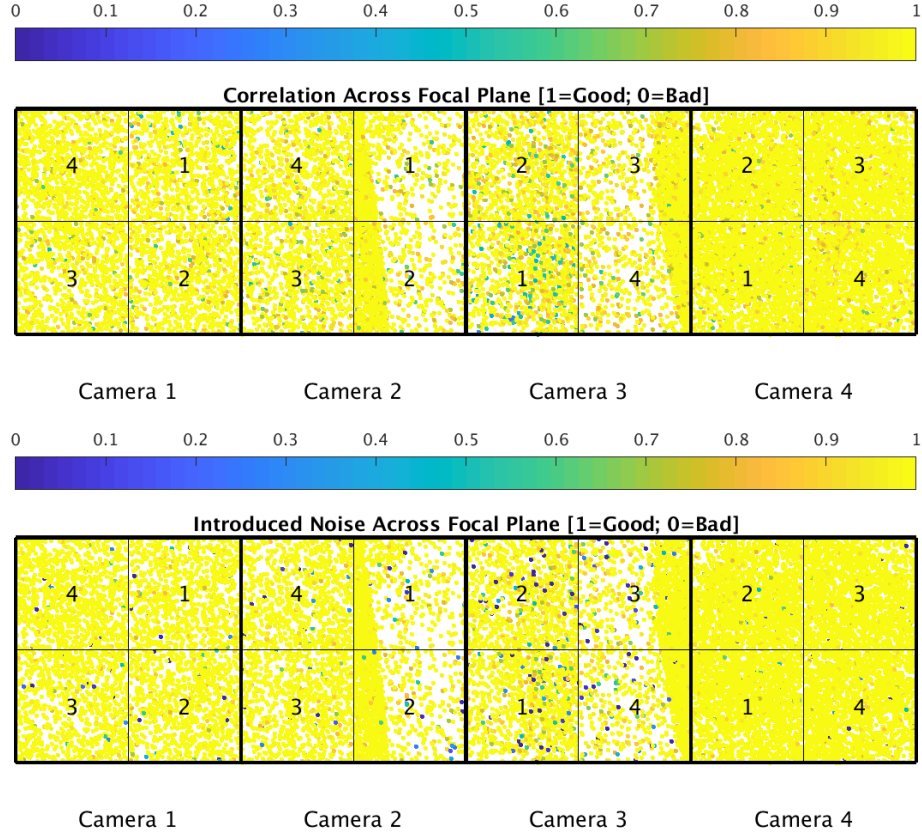
Figure 5: PDC residual correlation goodness metric (top panel) and PDC introduced noise goodness metric (bottom panel). The metric values are shown on a focal plane map indicating the camera and CCD location of each target. The correlation goodness metric is calibrated such that a value greater than 0.8 means there is less than 10% mean absolute correlation between the target under study and all other targets on the CCD. The introduced noise metric is calibrated such that a value greater than 0.8 means the power in broad-band introduced noise is below the level of uncertainties in the flux values.

with periods of increased pointing jitter.

The vertical histogram in the right panel of Figure 7 shows the distribution of transit depths derived from limb-darkened transiting planet model fits for TCEs. The model transit depths range down to the order of 100 ppm, but the bulk of the transit depths are considerably larger.

A search for additional TCEs in potential multiple planet systems was conducted in DV through calls to TPS. A total of 1299 TCEs were ultimately identified in the SPOC pipeline on 900 unique target stars. Table 4 provides a breakdown of the number of TCEs by target. Note that targets with large numbers of TCEs are likely to include false positives.
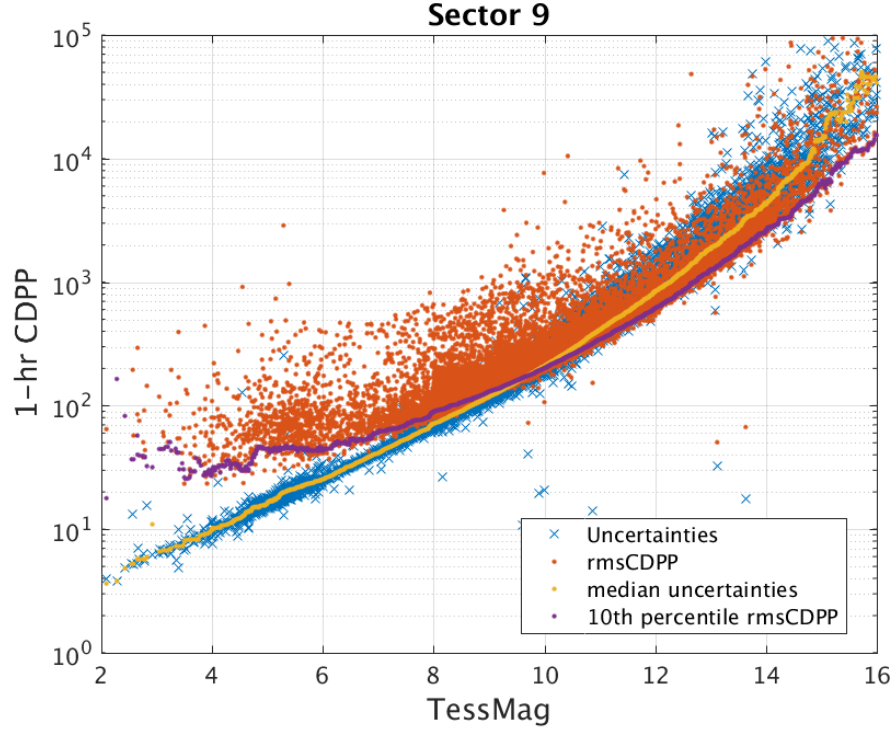
Figure 6: 1-hour CDPP. The red points are the RMS CDPP measurements for the 19996 light curves from Sector 9 plotted as a function of TESS magnitude. The blue x's are the uncertainties, scaled to 1-hour timescale. The purple curve is a moving 10th percentile of the RMS CDPP measurements, and the gold curve is a moving median of the 1-hr uncertainties.

Table 4: Sector 9 TCE Numbers

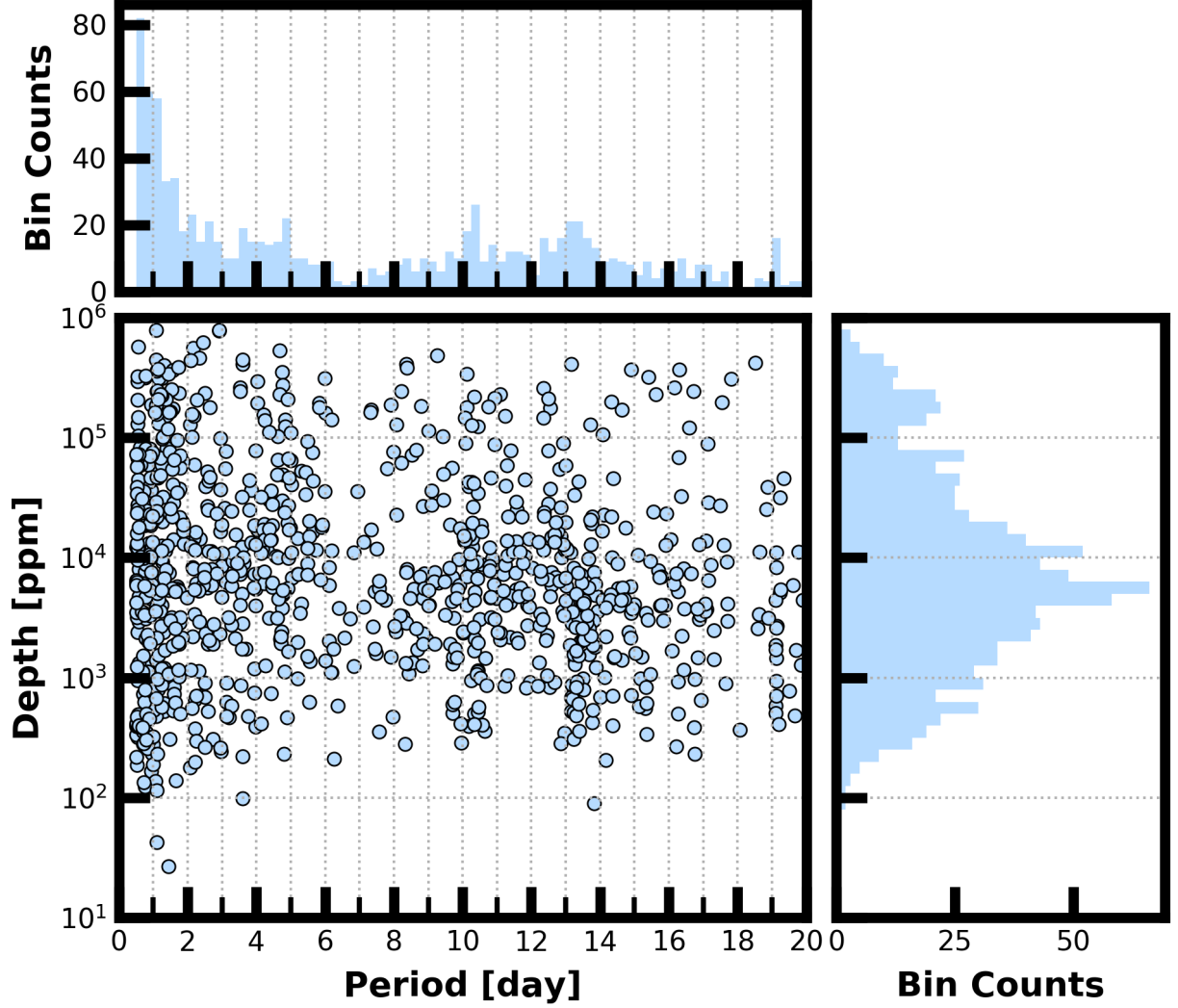| Number of TCEs	Number of Targets	Total TCEs
1	581	581
2	255	510
3	53	159
4	7	28
5	3	15
6	1	6
–	900	1299

Figure 7: Lower Left Panel: Transit depth as a function of orbital period for the 1299 TCEs identified for the Sector 9 search. For enhanced visibility of long period detections, TCEs with orbital period <0.5 days are not shown. Reported depth comes from the DV limb darkened transit fit depth when available, and when not available, the DV trapezoid model fit depth. Top Panel: Orbital period distribution of the TCEs shown in the lower left panel. Right Panel: Transit depth distribution for the TCEs shown in the lower left panel.
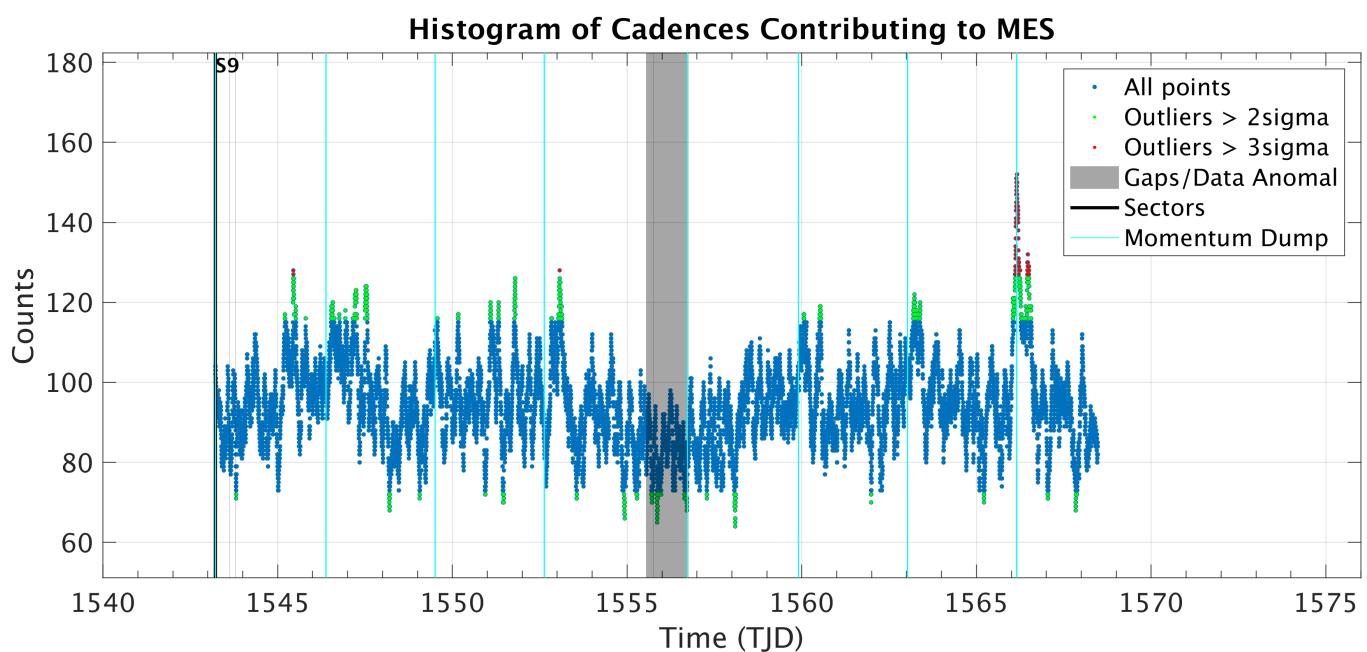
Figure 8: Number of TCEs at a given cadence exhibiting a transit signal. Isolated peaks are caused by a single event and result in spurious TCEs. The peaks typically align with pointing instabilities and strong background variations.

References

Jenkins, J. M. 2017, Kepler Data Processing Handbook: Overview of the Science Operations Center, Tech. rep., NASA Ames Research Center

Jenkins, J. M., Twicken, J. D., McCauliff, S., et al. 2016, in Proc. SPIE, Vol. 9913, Software and Cyberinfrastructure for Astronomy IV, 99133E

Li, J., Tenenbaum, P., Twicken, J. D., et al. 2019, *PASP*, 131, 024506

Twicken, J. D., Catanzarite, J. H., Clarke, B. D., et al. 2018, *PASP*, 130, 064502

Vanderspek, R., Doty, J., Fausnaugh, M., et al. 2018, TESS Instrument Handbook, Tech. rep., Kavli Institute for Astrophysics and Space Science, Massachusetts Institute of Technology

Acronyms and Abbreviation List

BTJD Barycentric-corrected TESS Julian Date

CAL Calibration Pipeline Module

CBV Cotrending Basis Vector

CCD Charge Coupled Device

CDPP Combined Differential Photometric Precision

COA Compute Optimal Aperture Pipeline Module

CSCI Computer Software Configuration Item

CTE Charge Transfer Efficiency

Dec Declination

DR Data Release

DV Data Validation Pipeline Module

DVA Differential Velocity Aberration

FFI Full Frame Image

FIN FFI Index Number

FITS Flexible Image Transport System

FOV Field of View

FPG Focal Plane Geometry model

KDPH Kepler Data Processing Handbook

KIH Kepler Instrument Handbook

KOI Kepler Object of Interest

MAD Median Absolute Deviation

MAP Maximum A Posteriori

MAST Mikulski Archive for Space Telescopes

MES Multiple Event Statistic

NAS NASA Advanced Supercomputing Division

PA Photometric Analysis Pipeline Module

PDC Pre-Search Data Conditioning Pipeline Module

PDC-MAP Pre-Search Data Conditioning Maximum A Posteriori algorithm

PDC-msMAP Pre-Search Data Conditioning Multiscale Maximum A Posteriori algorithm

PDF Portable Document Format

POC Payload Operations Center

POU Propagation of Uncertainties

ppm Parts-per-million

PRF Pixel Response Function

RA Right Ascension

RMS Root Mean Square

SAP Simple Aperture Photometry

SDPDD Science Data Product Description Document

SNR Signal-to-Noise Ratio

SPOC Science Processing Operations Center

SVD Singular Value Decomposition

TCE Threshold Crossing Event

TESS Transiting Exoplanet Survey Satellite

TIC TESS Input Catalog

TIH TESS Instrument Handbook

TJD TESS Julian Date

TOI TESS Object of Interest

TPS Transiting Planet Search Pipeline Module

UTC Coordinated Universal Time

XML Extensible Markup Language